

High Quality Appearance Models of Heart Sub-Components Based on MR Images

M. Wierzbicki, J. Moore, T. Peters
Imaging Research Laboratories, Robarts Research Institute
100 Perth Drive, PO Box 5015
London, ON, N6A 5K8, Canada

Abstract—High quality images have many uses, such as the testing of image processing algorithms and serving as templates for registration in image guided surgery. This work describes the creation of four high quality images or “appearance models”, for 1. Myocardium, 2. Right atrium and ventricle, 3. Left atrium and aorta, and 4. Epicardial surface. The appearance models are created by registering and averaging together a series of high-resolution MR images of the same volunteer. These are then corrected to represent the average shape as determined from MR data of ten other volunteers. Thus, we show how single volunteer imaging can be combined with image registration to generate average-shape appearance models with high resolution and signal-to-noise ratio. Our final data consist of four 3D average shape appearance models (each depicting one of the sub-heart components) with $1.5 \times 1.5 \times 1.5 \text{ mm}^3$ voxels and a signal-to-noise ratio increase of 6.6 versus raw data.

I. INTRODUCTION

Appearance and probabilistic models have been used in a variety of applications, including the development of an electrophysiological atlas of the deep brain to guide minimally invasive neurosurgery [1], the creation of a digital brain phantom designed for testing and development of image processing algorithms [2], and the segmentation of 4D cardiac MR images [3]. In the context of the work presented here, an *appearance model* (AM) is a high signal-to-noise ratio (SNR) and high resolution image, accurately depicting the 3D appearance of a given tissue or organ. A *probabilistic model* (PM) on the other hand, is an image containing the probability that a given tissue type is located at a specific point in 3D space. Therefore, the two models together contain information about the 3D appearance and the shape of a given tissue.

Recently, AMs and PMs were also developed for sub-heart components in order to segment 4D MR images [4]. The MR data used to generate these models was acquired slice-by-slice, with high resolution in-plane, and fairly low resolution out-of-plane (6 to 7 mm thick slices). The advantages of thick slice data are a relatively high SNR, short breath-hold duration, and short imaging time. As a result, images of many volunteers can be easily acquired and combined to create models that represent the *average shape* of the population. This is very important, since an AM representative of only one, possibly very uncommon

heart, is not desirable in image processing or image guided surgery applications. On the other hand, the obvious shortcoming of thick slice models is the lack of information in the out-of-plane direction.

Previously, we have shown how isotropic MR slices ($1.5 \times 1.5 \times 1.5 \text{ mm}^3$) could be acquired at the cost of SNR by increasing the breath-hold duration and imaging time. The decrease in SNR could then be compensated for by averaging images over different acquisition sessions [5]. This approach could be used to acquire images from different volunteers to create a high resolution, average shape AM. However, the imaging protocol requires long breath holds (~50 sec per slice), long imaging time (2.5 hrs per session), many imaging sessions (nine), and a significant amount of data processing. Realistically, this method can be performed on only one, very motivated volunteer; thus the resulting AM is representative of only a single heart.

In this work, we describe a method for correcting the shape of a high resolution, single-volunteer AM to be the average shape of the population. This is done by acquiring thick slice data from ten other volunteers to create a population PM for each of the four sub-heart components: 1. Myocardium (myo), 2. Right atrium and ventricle (RAV), 3. Left atrium and aorta (LAAo) and 4. Epicardial surface (epi). The four PMs are then used to modify the single-volunteer AM, creating four, *average shape* AMs, one for each heart component.

II. VOLUNTEER-SPECIFIC APPEARANCE MODEL

Our method for creating the high resolution AM of a single volunteer has been described previously [5]. In summary, raw images of the same volunteer were acquired over nine separate imaging sessions. An ECG gated protocol was used to separate the cardiac cycle into twenty time points, producing twenty 3D volumes per session. The imaging parameters were chosen so that all volumes had isotropic 1.5 mm voxels, and as a result, long breath-hold duration was required (approximately 50 sec). The raw volumes were corrected for breath-hold artefacts and re-arranged so that for each time point in the cardiac cycle, there were 45 volumes that were registered together and averaged (a theoretical increase in SNR of $\sqrt{45} \sim 6.7$). Thus, the initial AM is a 4D image consisting of twenty 3D volumes over the cardiac cycle, each with both high resolution and SNR. For further processing in this work, we

only use the mid-diastole 3D frame of the initial AM, and refer to it as AM_I .

For the shape correction calculation, a PM_I for each of the four sub-heart components was created as follows. First, the geometries of myo, RAV, LAAo, and epi were extracted using manual segmentation from AM_I . Each of the four resulting surfaces was then converted to an edge image, with values equal to unity for voxels intersecting the given surface, and zero elsewhere. These images were then blurred with a Gaussian filter ($\sigma = 2$ mm), resulting in four single-volunteer, probabilistic models: PM_I^{myo} , PM_I^{RAV} , PM_I^{LAAo} , and PM_I^{epi} .

III. AVERAGE SHAPE APPEARANCE MODELS

The following sections describe how images of other volunteers were used to create population PMs, and how these models were used to extract the average shape correction for AM_I . This important process ensures that the final AM is representative of the most common heart shape.

A. Image Acquisition

In total, ten healthy volunteers were imaged (3 female, 7 male), using a 1.5 T GE CVi scanner with ECG gating and the fast cine SPGR pulse sequence. This time, imaging parameters were modified to reduce the breath-hold duration and total scan time to a more reasonable 20 sec and 20 min respectively. This was achieved at the cost of image resolution (voxel size was $1.5 \times 6.0 \times 1.5$ mm³).

B. Population Probabilistic Models

The mid-diastole 3D volume of each volunteer was selected for the creation of the population probabilistic models specific to each of the four sub-heart components (PM_P^{myo} , PM_P^{RAV} , PM_P^{LAAo} , PM_P^{epi}). As before, the geometries of these components were extracted for each volunteer using manual segmentation. All of the volunteer images were then registered to a common target before the final PM_P^{myo} , PM_P^{RAV} , PM_P^{LAAo} , and PM_P^{epi} were computed. The global alignment was calculated between each volunteer *MR image* and AM_I using an affine transformation (T_G) taking into account 3D translations, rotations, scaling, and shearing. To take advantage of the high quality of AM_I , the transformation that aligns a given volunteer image (I_P) with AM_I was found instead by inverting the transform that registers AM_I to I_P . T_G was computed separately for each volunteer and each sub-heart structure by minimizing the following cost function using the downhill simplex algorithm:

$$C(T_G) = -NMI(T_G(AM_I), I_P, T_G(V)) + \alpha \cdot NND(T_G(P_{AM_I}), P_P) \quad (1)$$

The first term in the cost function is the negative normalized mutual information (-NMI) of the transformed AM_I , and the original volunteer image I_P , calculated over a volume of data surrounding the sub-heart structure being registered, $T_G(V)$. This term determines how similar the two images

are, and has previously been used in image registration [6]. The second term in (1) is the nearest-neighbor Euclidian distance (NND) between the transformed points on AM_I , P_{AM} (available from the manual segmentation), and a small number of user selected points on the surface of the same anatomy in the volunteer image, P_P . The purpose of this calculation is to aid the first term in overcoming the limited information available in the low resolution volunteer images. The contribution of both terms is controlled by the parameter α , which is set to 0.1.

Once the affine transformations for each sub-heart component of each volunteer are known, they are used to transform the 40 (four heart components \times ten volunteers) extracted surfaces into the AM_I coordinate system. The surfaces are then converted to edge images as described previously and filtered with a Gaussian filter ($\sigma = 2$ mm). The resulting filtered images are averaged over the ten volunteers, producing PM_P^{myo} , PM_P^{RAV} , PM_P^{LAAo} , and PM_P^{epi} .

C. Average Shape Correction

The correction that modifies AM_I to the average shape of the population is calculated using the four PM_I and four PM_P . This is achieved by non-linearly registering each PM_I to the corresponding PM_P , using a previously described free-form deformation algorithm based on minimizing the mean squared difference of two images [7]. The resulting non-linear mappings between each PM_I and PM_P are then applied to AM_I producing four *average shape* appearance models: AM^{myo} , AM^{RAV} , AM^{LAAo} , and AM^{epi} .

The entire process is repeated several times. At each iteration, all volunteer images are registered (affine) to the recently corrected appearance models AM^{myo} , AM^{RAV} , AM^{LAAo} , and AM^{epi} . The resulting transformations are used to create updated versions of PM_P^{myo} , PM_P^{RAV} , PM_P^{LAAo} , and PM_P^{epi} . A new average shape correction is calculated using the free-form deformation registration algorithm. The correction is applied to AM_I resulting in an even more average-shaped set of AM^{myo} , AM^{RAV} , AM^{LAAo} , and AM^{epi} .

IV. RESULTS AND DISCUSSION

In this work we have presented a method that combines specialized imaging techniques realistically applicable on only one volunteer with more generic image acquisitions to create four high quality, average shape AMs. In Fig. 1, we show the high SNR of our AM_I when compared to the raw data used to construct it. In fact, the actual increase in SNR due to averaging was 6.6, very close to the theoretically expected value of $\sqrt{45} \sim 6.7$. This comes at a cost of a small amount of blurring in AM_I , mostly from interpolating original raw data after registration during the averaging process. However, we found the blurring to be insignificant compared to the reduction in noise. Fig. 1 also shows the high resolution of AM_I . The $1.5 \times 1.5 \times 1.5$ mm³ isotropic

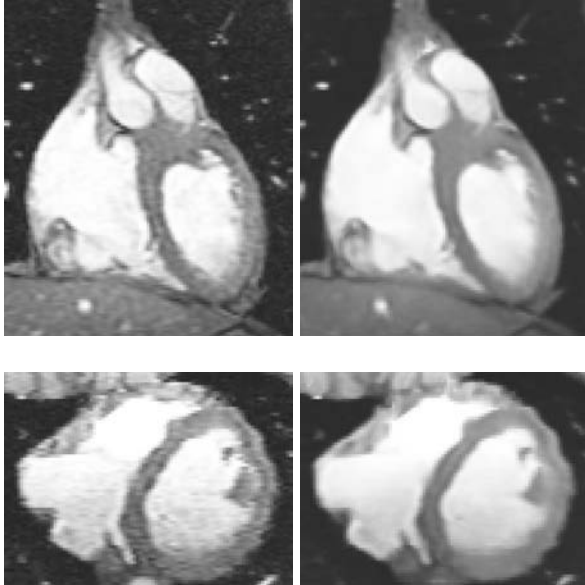


Fig. 1: Corresponding coronal (top) and axial (bottom) slices from one of the raw images used to make AM_I (left), and AM_I itself (right). Notice the increase in SNR in the images on the right.

voxels allow the volume to be viewed from any angle without the stair-step artefact observed in thick slice data.

Fig. 2 shows the manually extracted surface models from AM_I . These models were used to make PM_I^{myo} , PM_I^{RAV} , PM_I^{LAAo} , and PM_I^{epi} . Similar models were extracted for each volunteer image in order to construct PM_P^{myo} , PM_P^{RAV} , PM_P^{LAAo} , and PM_P^{epi} .

The effects of averaging the shape of the appearance models can be seen qualitatively in Fig. 3. In the first column are the four sub-heart component probabilistic models obtained without any shape correction of AM_I . The arrows point to some areas of the models where the probability is diffuse indicating two things: 1. Large variation in the shape of these areas of the heart over the volunteer population, and 2. Difficulties in registering volunteer data to the single volunteer-specific AM_I . Once the average shape correction is computed and applied to AM_I , the probability models become slightly tighter as shown in the second column. Since the volunteer population is exactly the same as before, the tightening in probability models indicates more accurate registration of volunteer data to the corrected AM_I . This in turn indicates that AM_I is converging toward the correct average shape in the dataset. In the third column we see the effects of iterating through the shape correction process once more. This time, the tightening of the probabilistic models is not as pronounced, as the appearance models have already approached the true average shape. In fact, we found that iterating the method more than twice was not worth the investment in computation time, since further changes to the shape of AM were insignificant.

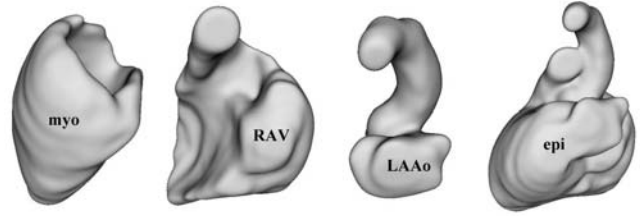


Fig. 2: Surface models manually extracted from AM_I .

The quantitative effects of averaging the shape of AM_I can be seen in Table I. The first row of data gives the average of the RMS Euclidean distance between closest points on the surfaces manually extracted from AM_I , and the surfaces extracted manually from the ten volunteers following affine registration to AM_I (no shape averaging correction). The epi model is the most variable between volunteers and the most difficult to register as indicated by the large mean distance and standard deviation. This is not surprising, since it spans a variety of different locations in the heart, with the most possibility for variability between volunteers. The second and third rows of the table contain the mean surface distances after the shape of AM_I is corrected through one and two iterations. The improvement in the ability to register (affine) volunteer data to the corrected AM_I is most pronounced in the first iteration, with almost no improvement in the second. Overall, the improvement is significant but small, indicating that by chance, the shape of the volunteer heart chosen for AM_I creation was already somewhat average when compared to the shapes of the other ten volunteer hearts.

This paper describes the creation of appearance models of the sub-heart anatomy for the purpose of testing image processing algorithms and for specific applications in image guided surgery of the heart. The four appearance models created (AM^{myo} , AM^{RAV} , AM^{LAAo} , and AM^{epi}) are of a higher than normal resolution in cardiac MR imaging especially in the out of plane direction (1.5 mm isotropic voxels). The SNR of the appearance models is 6.6 times higher than the raw data used to create them, and the shape of the heart is corrected to be the average population shape as determined from MR images of ten other volunteers. In the future, we will extend this method to create a 4D average shape AM. Also, we plan to use the AMs in automatic segmentation of patient images, for the purpose of planning and guiding minimally invasive cardiac surgery.

TABLE I

AVERAGE RMS EUCLIDEAN DISTANCE BETWEEN CLOSEST POINTS ON AM_I SURFACE MODELS AFTER THEY HAVE BEEN TRANSFORMED BY THE AVERAGE SHAPE CORRECTIONS AND THE SURFACE MODELS OF THE VOLUNTEERS AFTER AFFINE REGISTRATION TO THE CORRECTED AMS.				
Iterations	Average RMS \pm STD Euclidean Distance (mm)			
	myo	RAV	LAAo	epi
0	3.01 \pm 0.35	3.23 \pm 0.64	3.26 \pm 0.55	3.82 \pm 0.98
1	2.83 \pm 0.36	2.93 \pm 0.52	2.47 \pm 0.41	3.45 \pm 0.92
2	2.85 \pm 0.34	2.88 \pm 0.52	2.40 \pm 0.41	3.45 \pm 0.90

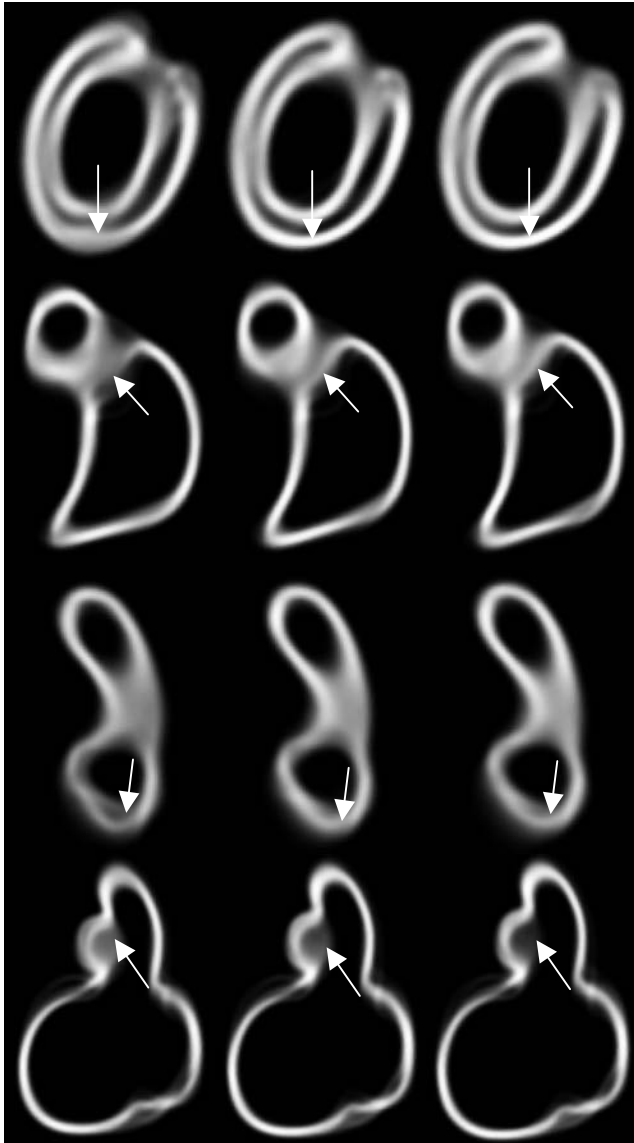


Fig. 3: Rows: Coronal slices from PM_p^{myo} , PM_p^{RAV} , PM_p^{LAAo} , and PM_p^{epi} population PMs. Columns: Number of iterations of the shape averaging method starting with 0 on the left, 1 in the middle, and 2 on the right. Note the tightening of the probability distribution with increasing iterations.

ACKNOWLEDGMENT

The authors would like to acknowledge Atamai, Inc. (www.atamai.com) for the visualization/interaction software, and Dr. Maria Drangova and Rhonda Walcarius for imaging help. This work was supported in part by grants from the Canadian Institutes of Health Research (MOP 14735), Canadian Heart and Stroke Foundation (NA 4755), Ontario Consortium for Image Guided Surgery and Therapy, Canadian Foundation for Innovation, Ontario Innovation Trust, National Science and Engineering Research Council of Canada, and the University of Western Ontario.

REFERENCES

- [1] K. Finnis, Y. Starreveld, and T. Peters, "A 3D database of deep brain functional anatomy and its application to image guided neurosurgery," in *Medical Image Computing and Computer-Assisted Intervention* (MICCAI 2000), 2000, pp. 1-8.
- [2] D. Collins, A. Zijdenbos, V. Kollokian, J. Sled, N. Kabani, C. Holmes, and A. Evans, "Design and construction of a realistic digital brain phantom," *IEEE Trans. Med. Imaging*, vol. 17, no. 3, 1998, pp. 463-468.
- [3] M. Lorenzo-Valdés, G. Sanchez-Ortiz, A. Elkington, R. Mohiaddin, and D. Ruckert, "Segmentation of 4D cardiac MR images using a probabilistic atlas and the EM algorithm," *Med. Image Anal.*, vol. 8, 2004, pp. 255-265.
- [4] J. Lötjönen, S. Kivistö, J. Koikkalainen, D. Smutek, and K. Lauerma, "Statistical shape model of atria, ventricles and epicardium from short- and long-axis MR images," *Med. Image Anal.*, vol. 8, 2004, pp. 371-386.
- [5] J. Moore, M. Drangova, M. Wierzbicki, J. Barron, and T. Peters, "A high resolution MRI heart model," submitted to *Medical Image Computing and Computer-Assisted Intervention* (MICCAI 2005), 2005.
- [6] C. Studholme, D. Hill, and D. Hawkes, "An overlap invariant entropy measure of 3D medical image alignment," *Pattern Recognit.*, vol. 32, no. 1, 1999, pp. 71-86.
- [7] M. Wierzbicki, M. Drangova, G. Guiraudon, and T. Peters, "Validation of dynamic heart models obtained using non-linear registration for virtual reality training, planning, and guidance of minimally invasive cardiac surgeries," *Med. Image Anal.*, vol. 8, 2004, pp. 387-401.